# Structural Determination of Copper Species on the Alumina-Supported Copper Chloride Catalyst: A Detailed EXAFS Study

**C. Prestipino, S. Bordiga, and C. Lamberti***

*Department of Inorganic, Physical and Materials Chemistry, University of Turin, Via P. Giuria 7, 10125 Torino, Italy, and INFM UdR Torino-Università*

**S. Vidotto, M. Garilli, B. Cremaschi, A. Marsella, and G. Leofanti**†

*European Vinyls Corporation Italia, EVC Technological Centre, Via della Chimica 5, 31075 Porto Marghera, Venezia, Italy*

**P. Fisicaro, G. Spoto, and A. Zecchina**

*Department of Inorganic, Physical and Material Chemistry, University of Turin, Via P. Giuria 7, 10125 Torino, Italy*

*Received: November 20, 2002; In Final Form: March 17, 2003*

We present a methodology that allows us to extract quantitative information from EXAFS data collected on complex samples where the absorbing species is present in more than one phase. We have chosen as our case study the $CuCl_2/Al_2O_3$ material, which represents the basic catalyst for the ethylene oxychlorination reaction (a fundamental intermediate step in PVC production). In previous studies [*J. Catal.* **2000**, *189*, 91, and *J. Catal.* **2000**, *189*, 105], it has been shown that three different copper species are present on $CuCl_2/Al_2O_3$—a Cu-aluminate phase, a highly dispersed copper chloride phase, and an aggregated paratacamite ($Cu_2(OH)_3Cl$) phase, whose relative fraction depends on copper loading, sample aging, and heating conditions. In this work, we extract from the EXAFS spectra the fraction of the three phases on a quantitative ground. A study of the corresponding XANES spectra allows us to qualitatively support the EXAFS results. This methodology represents a generalization of the standard EXAFS procedure that can be of general interest in all cases where more than one phase is present on the sample.

## 1. Introduction

Nowadays, almost all the world production of vinyl chloride is based on cracking of 1,2-dichloroethane, which in its turn is produced by catalytic oxychlorination of ethylene with hydrochloric acid and oxygen,[1] and follows the reaction path:

$$C_2H_4 + 2HCl + {}^1/_2O_2 \rightarrow C_2H_4Cl_2 + H_2O \qquad (1)$$

The reaction is performed at 490−530 K and 5−6 atm (1 atm $\approx 1.01 \times 10^5$ Pa) using both air and oxygen in fluid or fixed bed reactors.[2] Commercial catalysts are produced by impregnation of alumina with $CuCl_2$ (4−8 wt % Cu). Also, Other chlorides (mainly alkaline or alkaline earth chlorides) in a variable concentration[1,3] are also added in order to improve the catalytic performances, making the catalyst more suitable for the use in industrial reactors.[1,3,4]

Despite the great number of investigations since the seventies,[5−18] the problem of identifying the structure of all the copper species present on the catalyst has been debated for 30 years and several conflicting conclusions have been drafted. Even if the existence of some different families of Cu compounds emerges from most of the quoted works, when an attempt is made to compare quantitatively the relative fractions, conflicting results are systematically obtained. The reason for such a debated situation has been, at least partially, explained in three works[19−21] that appeared in year 2000, where it has been demonstrated that the chemical nature of the copper species present on the catalyst depends on four main factors: (i) copper content, (ii) surface area of the $\gamma$-$Al_2O_3$ support, (iii) catalyst aging, and (iv) activation temperature. As a consequence, comparison among results coming from different articles can be made only if the four factors have been clearly defined in the corresponding Experimental Sections. If not, misleading comparison can be obtained.

In such works,[19−21] a systematic study on a set of $CuCl_2/Al_2O_3$ catalysts prepared in a wide range (0.25−9 Cu wt %) of Cu concentration has been reported as a function of both aging time and thermal activation up to the typical oxychlorination temperature (500−550 K). As far as freshly prepared catalysts are concerned,[19] it has been demonstrated that only two copper phases are present: (i) a phase with copper content lower than 0.95 wt % Cu per 100 $m^2$ support, the formation of surface aluminate taking place where the copper ions are surrounded only by oxygen ligands which form a tetragonally distorted octahedral environment (5 oxygen ligands at 1.94 Å); (ii) once that the adsorptive capacity of alumina surface is exhausted, copper chloride precipitates directly from the solution with the formation of highly dispersed $CuCl_2 \cdot 2H_2O$. It has been demonstrated that the surface Cu-aluminate is stable under both

* Author to whom correspondence should be addressed. Fax: +39-011-6707855. E-mail: carlo.lamberti@unito.it.

† Consultant. Present address: Via Firenze 43, 20010 Canegrate, Milano, Italy.

10.1021/jp027507b CCC: $25.00 
Published on Web 05/02/2003

aging and heating treatments, while hydrated $CuCl_2$ undergoes a slow hydrolysis process resulting in the formation of crystalline paratacamite ($Cu_2(OH)_3Cl$), an insoluble copper hydroxochloride.[20] The $CuCl_2 \cdot 2H_2O/Cu_2(OH)_3Cl$ ratio decreases with increasing aging time. The HCl released during the hydrolysis is not lost by the catalyst but reacts with alumina with formation of >Al−Cl species, ensuring a Cl/Cu ratio of 2 throughout the aging process. Under heating, the alumina partially releases the chlorine fixed to the surface, resulting in the reverse transformation of paratacamite into copper chloride (anhydrous in this case).[19−21] As a consequence of these findings, it has been concluded that, in the oxychlorination reaction conditions, paratacamite is absent and only surface aluminate and copper chloride (or products arising from the interaction of these compounds with reactants or reaction products) are present in the catalyst.[19−21] Finally, it has been shown that the surface copper aluminate is inactive and that ethylene conversion, determined with a conventional pulse reactor, is proportional to the amount of copper chloride, which has thus been identified as the active phase.[20,21]

In three successive works the interaction of the catalyst with the oxychlorination reagents ($C_2H_4$, $O_2$, and HCl) has been in-situ investigated.[22−24] On a computational ground, the work of Neurockn et al.[25] has recently reported a study on the ethylene chemisorption on model copper chloride [$Cu_xCl_y$,$Cu_xCl_y(OH)_z$] and supported copper chloride [$Cu_xCl_y(OH)_z/Al_r(OH)_s$] clusters, examined using spin-polarized gradient corrected density functional theory.

In this paper we report a detailed EXAFS study aimed to quantify the amount of copper aluminate, paratacamite and of $CuCl_2$ (hydrated or anhydrous) present on the aged catalysts as a function of the Cu loading and of the thermal treatment up to 500 K. In this work, we present a methodology that allows us to extract quantitative information from EXAFS data collected on complex samples such the $CuCl_2/\gamma$-$Al_2O_3$ system. Similar approaches have already been proposed, for example, for nanometer-scale metallic cluster in the paper by Moonen et al.,[26] and for copper and silver hosted in different cationic sites of Y zeolite by our group.[27,28]

## 2. Experimental Section

Investigated samples are characterized by a Cu loading ranging from 1.4 to 9.0 wt % and were prepared by impregnation of $\gamma$-alumina (Condea Puralox SCCa 30/170, surface area: 168 $m^2\ g^{-1}$, pore volume: 0.50 $cm^3\ g^{-1}$) with an aqueous solution of $CuCl_2 \cdot H_2O$ following the incipient wetness method.[19] According to the convention adopted in refs 19,20, the copper content is used to identify the samples: for example Cu9.0 indicates the sample containing 9.0 wt % Cu.

X-ray absorption measurements were carried out using synchrotron radiation of the EXAFS13 station at LURE (Orsay, France) during experiment CK017-00.[29] Extended X-ray absorption fine structure (EXAFS) measurements were carried out in transmission mode, using air-filled ionization chambers for both incident and transmitted beams. The former was monochromatized using a Si(111) channel-cut monochromator. Four EXAFS spectra have been collected in the same experimental conditions with a sampling step of 2.0 eV/point and an integration time of 2 s/point. A single XANES spectrum was acquired for each sample, with a sampling step of 0.5 eV/point and an integration time of 2 s/point. Extracted $\chi(k)$ have been averaged before the EXAFS data analysis as detailed in ref 30. Standard deviation, calculated from the four EXAFS spectra, was used as an estimate of the statistical noise for the evaluation of the error associated with each structural parameter. Experimental $\chi(k)$ was extracted from absorption data as described in details in ref 30, with the only exception that in this case a 6th degree polynomial fit was used to estimate the atomic-like contribution. The $k^3$-weighted $\chi(k)$ were Fourier transformed over a Kaiser window, with $\tau = 2.5$. Main contributions to the Fourier transform modulus were filtered in order to obtain the Cu-nearest neighbor shell. The so obtained filtered contributions were analyzed using programs developed by Michalowicz,[31] following standard procedures.[32] The Cu−Cl and Cu−O contributions, in filtered EXAFS spectra, have been modeled using phase shift and amplitude functions extracted from anhydrous $CuCl_2$[33] and from the $Cu_2O$[34] model compound, respectively.

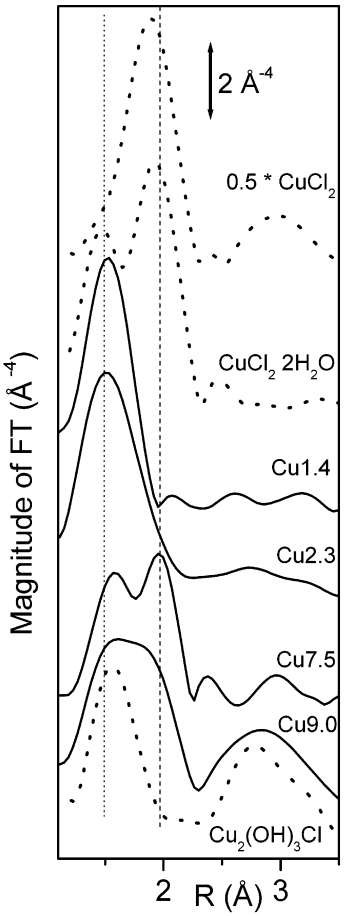


**Figure 1.** $k^3$-weighted, phase-uncorrected, FT of the EXAFS signals of the different samples aged about 6 months in air; from top to bottom: anhydrous $CuCl_2$, hydrated $CuCl_2$, Cu9.0, Cu7.5, Cu2.4, Cu1.4, and paratacamite (model compounds reported for comparison). The vertical dotted and dashed lines indicate approximately the typical Cu−O and Cu−Cl bond lengths.

The EPR spectrum of a sample characterized by a very low Cu content (Cu0.04) has been measured at liquid nitrogen temperature on a Varian E 109 spectrometer equipped with a dual cavity and operating in the X band. Varian Pitch was used as a reference for the calibration of $g$ values. Before cooling, samples were evacuated at RT up to $10^{-3}$ Torr (1 Torr = 133.3 Pa).

## 3. Results

Figure 1 reports the $k^3$-weighted, phase uncorrected, FT of the different catalysts (6 months aged) as a function of the increasing Cu loading. For comparison, also the corresponding FT of anhydrous and hydrated $CuCl_2$ and of paratacamite model

compounds are reported (dotted spectra). Anhydrous $CuCl_2$ shows a single peak at 1.88 Å (due to 4 Cl at 2.26 Å[33]), hydrated $CuCl_2$ shows two distinct peaks at 1.48 and 1.92 Å (due to 2 O 1.94 Å, and to 2 Cl at 2.28 Å[35]), while paratacamite shows a broad peak at 1.55 Å (due to a convolution of O in the 1.98−2.10 Å range[36]).

Cu1.4 catalyst shows only a single peak in the region of Cu−O distances (1.53 Å), which has been previously interpreted in terms of a dispersed surface aluminate phase,[19] in agreement with quantitative results from several other techniques. Conversely, catalyst Cu9.0 exhibits a much broader first shell peak, clearly shifted at higher *R* values (maximum at 1.63 Å and shoulder at 1.85 Å), indicating a coexistence of both Cu−O and Cu−Cl contributions. A relevant second shell peak (maximum at 2.85 Å) is also evident. Cu2.3 and Cu7.5 catalysts are intermediate between Cu1.4 and Cu9.0. The former show a first shell peak that begins to have an evident asymmetric tail in the high *R* region due to a small fraction of Cu−Cl contributions, the latter exhibit two nearly resolved peaks centered at 1.58 and 1.96 Å, respectively.

Figure 1 shows the coexistence of more than one contribution. At the increasing of Cu loading, the increase of the Cu−Cl contribution is parallel to the decrement of the Cu−O one. This fact is caused by two concomitant effects: (i) the decrement of the relative contribution of the aluminate phase, going from 100% for the Cu1.4 sample to 18% for that of Cu9.0; (ii) a less pronounced contribution of the oxygen of the paratacamite phase whose formation speed is lowered by moving from Cu2.4 to Cu9.0 samples.[20]

Quantitative results cannot be safely extracted with the typical EXAFS analysis procedure from high Cu loaded samples (Cu9.0, Cu7.5, Cu2.4) because the signal is formed by the overlap of different contribution coming from different scattering atoms located at different distances in three different phases (surface aluminate, $CuCl_2 \cdot H_2O$, and paratacamite). This means that the broad first shell peak extending into the 0.82−2.3 Å phase uncorrected range, receives a contribution from oxygen atoms of the surface aluminate, at 1.92 Å,[19] of the paratacamite in the range between 1.98 and 2.11 Å,[36] and of hydrated copper chloride at 1.95 Å, where also chlorine atoms at 2.29 Å are present.[37]

Figure 2 reports the evolution of the first shell FT signal of Cu7.5 catalyst after several steps of thermal activation: RT, 393, and 473 K. At RT, the Cu7.5 sample shows 2 peaks, ascribed to a coexistence of both Cu−O and Cu−Cl contributions. The sample activated at 393 K is characterized by a single peak at 1.85 Å, and a tail at 1.63 Å. Only the sample activated at 473 exhibits a single peak at 1.85 Å, characteristic of Cu−Cl contributions, while the previous two spectra have a significant component ascribed at the C−O contribution. As for the spectra reported in Figure 1, also for those reported in Figure 2 a convectional EXAFS analysis cannot be performed because of the too elevated number of the parameter that has to be optimized.

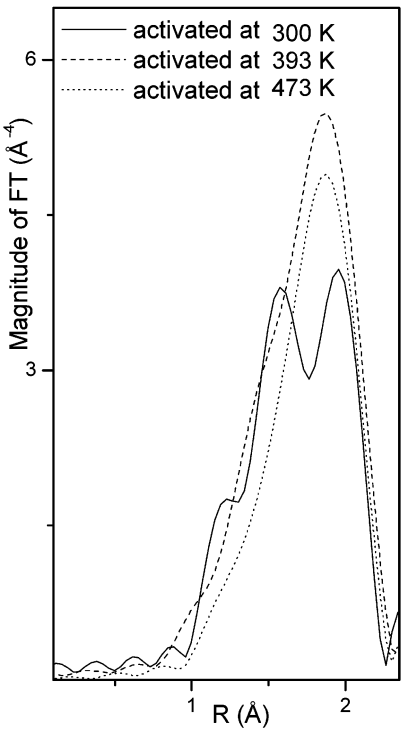


**Figure 2.** $k^3$-weighted, phase-uncorrected, FT of the EXAFS signals of Cu7.5 catalyst after activation at 300, 394, and 473 K (full, dashed, and dotted lines, respectively).

## 4. Discussion

**4.1. On the Research of an EXAFS Analysis Approach.** A conventional EXAFS analysis is usually performed on sample with a single chemical species in the sample, and so all the absorbing atoms have the same local coordination. In this case, the value obtained by the best-fit procedure of EXAFS data is an evaluation of the real structural parameters around the absorber atom.

If more than a chemical species is present in the sample, the EXAFS signal is the sum of signals corresponding to all phases. In such a case, the fit must be performed by using a number of theoretical contributions equal to the number of chemical species present in the sample. In this paper, we shall limit the discussion to the first coordination shell analysis of each phase. So, if *F* is the number of phases, the model will include *F* different first shell signals, where *N*, *R*, $\sigma$, and $\Delta E$ should be, in principle, optimized.

Under these assumptions, the distances and the Debye−Waller factors obtained by the best-fit procedure are still correct evaluations of the value of these parameters for each phase in the sample. Conversely, the coordination number obtained by the fit does not represent the number of atoms surrounding the absorbing atom in each phase, but it is only proportional to it according to the following relationship:[27,28]

$$N_{\mathrm{fit}\,i} = N_i\, x_i \quad i = 1 \ldots F \tag{2}$$

where $N_i$ and $N_{\mathrm{fit}\,i}$ are the real coordination number in the *i*th phase and that one obtained by the best fit procedure respectively, while $x_i$ is the atomic fraction of the of the absorber in the *i*th phase.[38]

It is evident that the number of fitting parameters rapidly increases with *F*. So, such an approach can be successfully pursued only if severe constraints can be imposed on several parameters by information coming from other independent techniques. On this ground, the structural hypothesis planed out by Leofanti et al.[19,20] are the ideal starting point for the application of the methodology described above. In high-Cu-loaded sample, up to three phases are present: (1) Cu aluminate, (2) copper chloride, and (3) paratacamite. For each of the three phases, we will now proceed to fix all possible EXAFS parameters on the basis of the knowledge of the material achieved up to now.

On the basis of its remarkable stability to aging and thermal treatments,[19,20] we can assume that the relative contribution of the aluminate phase remains the same in all samples. This means

that, once a careful one-shell fit will be done on sample Cu1.4 (containing only this phase), the obtained $R$ and $\sigma$ values can be used as fixed parameters for the other samples. The same holds for the coordination once it will be weighted by the corresponding $x_{\text{aluminate}}$ value (2). So only $\Delta E$ has to be optimized for this phase, reflecting the fact that the estimation of $E_0$ can be different for each phase.

For the contribution simulating the anhydrous copper chloride[39] phase like the previous phase, $\Delta E_0$ is free to vary for the same reason described before, while the other structural parameters follow a different strategy for the fit optimization. The copper chloride present on the catalyst is extremely dispersed;[22] this suggests that the local environment around copper atoms can be slightly different from the $CuCl_2$ bulk. In particular, a larger Debye−Waller factor, resulting from heterogeneity of the particles dispersed on the catalyst, is expected. Instead, the number of ligands in the first shell must remain 4.

For the contribution representing the paratacamite phase, we have optimized $\Delta E_0$ and $N_{\text{fit}}$ only—the former for the reason illustrated above and the latter in order to estimate the fraction of paratacamite present on the sample. Conversely, the structural parameter has been fixed because the XRD measures[20] have proved that paratacamite is present in the sample in crystalline form and so the local environment is equal to the model compound used to extract phase and amplitude (vide infra, Section 4.3).

As a result, the total number of optimized parameters is seven: $\Delta E$ for the three phases, $N_{\text{fit}}$ for $CuCl_2$ and paratacamite, and $R$ and $\sigma$ for $CuCl_2$

**4.2. Optimization of the EXAFS Signal of the Surface Aluminate Phase.** To apply the EXAFS analysis criteria described before, we need to obtain the most accurate fit for the sample Cu1.4, where copper is present as aluminate phase only. On these grounds, the fit is not made in order to obtain structural information regarding the present phase (known by hypothesis), but its aim is to reproduce the experimental signal as closely as possible. The better the experimental signal of the Cu1.4 sample is reproduced, the better the contribution of the aluminate phase in the highly loaded samples will be estimated.

As far as the Cu1.4 sample is concerned, we know that Cu(II) ions are hosted in the octahedral surface vacancies of $\gamma$-$Al_2O_3$.[19−21] A satisfactory EXAFS fit was obtained by Leofanti et al.[19] on a sample of Cu1.4 by optimizing $N$, $\sigma$, the Cu−O distance $R$, and $\Delta E$. The validity of this model is further supported by an independent EPR experiment, performed on a sample with a very low copper content (Cu0.04), to minimize spin−spin relaxation phenomena and to increase the resolution of the hyperfine components of the experimental data. Figure 3 reports the experimental EPR spectrum (upper curve), which is typical of cupric ions in axial symmetry ($g_{xx} = g_{yy} \equiv g_{//}$ and $g_{zz} \equiv g_{\perp}$). In both components, the splitting into quartets, a result of the hyperfine interaction between the unpaired electron and the copper nucleus [both $^{63}$Cu and $^{65}$Cu nuclei have a 3/2 nuclear spin[40]], is clearly visible. The experimental signal has been successfully simulated as the superimposition of two very close axial contributions (lower curve). The first family (60% of the total signal) of cupric sites is characterized by the following g and hyperfine tensors: $g_{//}^1 = 2.3344$, $g_{\perp}^1 = 2.0667$, and $A_{//}^1 = 140$ G, $A_{\perp}^1 = 11.975$ G, being the second family (40% of the total signal) characterized by $g_{//}^2 = 2.3043$, $g_{\perp}^2 = 2.0587$, and $A_{//}^2 = 160$ G, $A_{\perp}^2 = 22.914$ G.

On the basis of what was learned from the EPR study, here we report an improved EXAFS fit of the Cu-aluminate phase (Figure 4). The closeness of the EPR parameters of the two

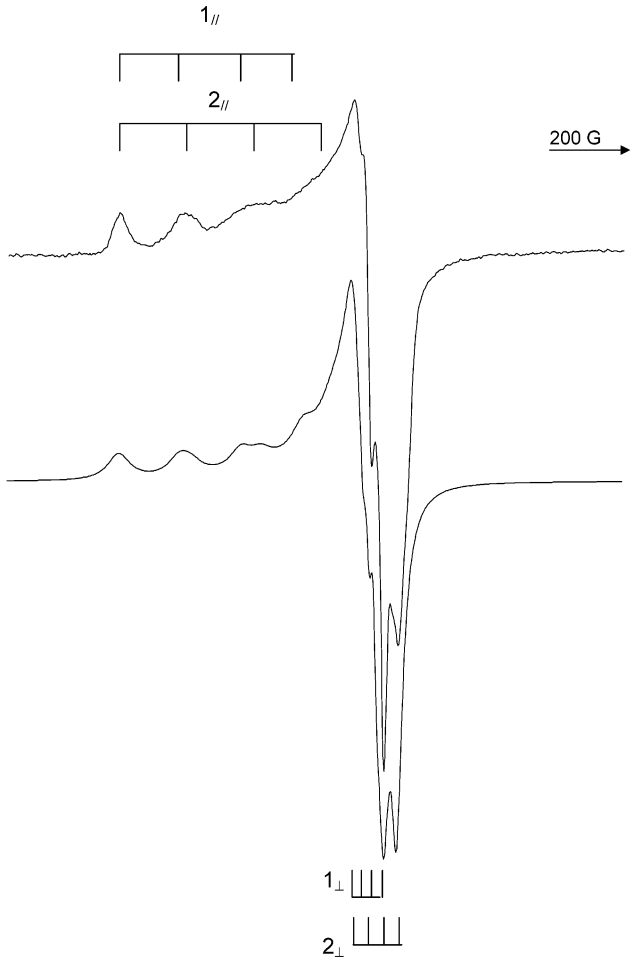


**Figure 3.** Experimental (collected at liquid nitrogen temperature, upper curve) and simulated (lower curve) EPR signal of the Cu0.04 sample. The simulated spectrum has been obtained as the superposition of two axial signals. The first signal, representing 60% of the total signal, is characterized by the following g and hyperfine tensors: $g_{//}^1 = 2.3344$, $g_{\perp}^1 = 2.0667$, and $A_{//}^1 = 140$ G, $A_{\perp}^1 = 11.975$ G, while for the second signal we have $g_{//}^2 = 2.3043$, $g_{\perp}^2 = 2.0587$, and $A_{//}^2 = 160$ G, $A_{\perp}^2 = 22.914$ G. Quartets indicate the position of the single hyperfine components of the simulated spectrum: the symbols $1_{//}$, $2_{//}$, $1_{\perp}$, and $2_{\perp}$ refer to the parallel and perpendicular components of families 1 and 2 of Cu(II) species.

sites means that we are dealing with two families of $Cu^{2+}$ surface sites characterized by a very similar axial environment, i.e. having four planar and one axial oxygen ligand in their first coordination sphere. The improved EXAFS fit has so been obtained by fixing $N$ at 5 (the expected coordination number of a surface octahedral cation) but optimizing also the electron mean free path parameter $\gamma$ that moves from the arbitrarily fixed value of $\gamma = 1.0$ to 0.7. The fit, although improved with respect to that presented in ref 19, does not present, within the experimental errors, any significant variation of the structural parameters. The optimized $R_{\text{Cu−O}}$ distance is now slightly stretched ($1.94 \pm 0.01$ Å) with respect to the value reported in ref 19: $1.92 \pm 0.02$ Å. It is interesting to note that 1.94 Å is exactly half of the O−O distance existing between each couple of oxygen atoms diametrically opposite in an octahedral cationic site of the $\gamma$-$Al_2O_3$ spinel structure.[41] It is finally worth noticing that, if $N$ is successively released, it converges to a value of 4.98.

**4.3. Simulation of the EXAFS Signal Coming from Paratacamite.** The paratacamite has a very complex structure in which the copper is present in four different equal populated

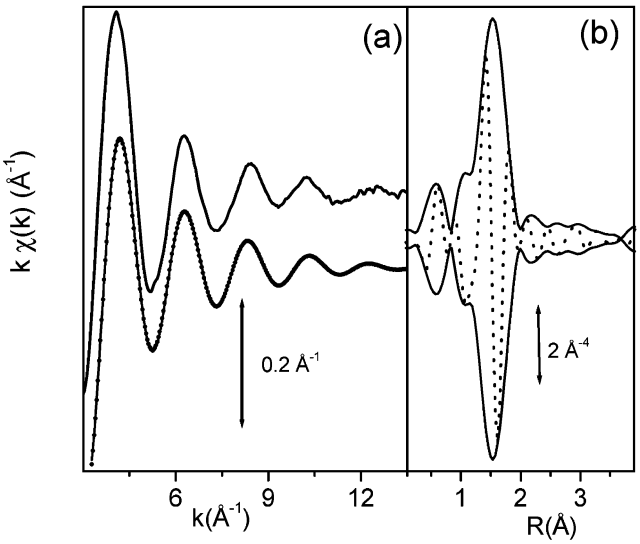


**Figure 4.** (a) From the top to the bottom: raw EXAFS data, first shell filtered data in scattered dots, and superimposing best fit (full line) obtained for the sample Cu1.4. (b) $k^3$-weighted, phase-uncorrected, FT of the raw EXAFS signal reported in part (a): modulus (full line) and imaginary part (dotted line).

sites, where it is coordinated both with O and Cl atoms at different distances. This complexity made the simulation of each single Cu−O and Cu−Cl distance to the overall EXAFS signal of paratacamite very difficult and hardly affected by correlation problems. This holds for paratacamite itself as a pure phase; in the here-discussed catalysts, the presence of other phases prevents any attempt to follow this route. With the aim of this work being the estimation of the fraction of the different phases present in the catalyst, another approach must be utilized for the reproduction of the signal of paratacamite.

Starting from the Fourier transformation of the overall EXAFS signal of the paratacamite model compound, the inverse FT, computed in the 1.20−1.97 Å range (see vertical arrows in Figure 5a), has been performed. This results in the filtered $\chi(k)$ function reported in Figure 5b, representing the sum of the contribution of all the atoms in the first shell around copper in the four different crystallographic sites, already correctly weighted.

The so-obtained signal, now can be used for the extraction of "fictitious" phase and amplitude, which reproduce the overall first shell signal of paratacamite. When extraction of phase and amplitude from model compounds has been performed, the process needs to provide the structural parameters that characterize the local environment around the absorber atoms. Normally, the model compounds are chosen with the absorber present in only one site with a homogeneous environment. In this case where more than one site will be present, the structural parameters for extraction have to be "fictitious", so we have chosen $R = 2$ Å, as average first shell distance, and for $N = 1$. When such phases and amplitudes are used to simulate the paratacamite contribution of one sample, the optimized $N_{fit}$ will directly result in the fraction of paratacamite present on the catalyst, while $R$ will be fixed to 2 Å.

**4.4. EXAFS Data Analysis of the Catalysts Activated at RT.** The systematic use of analysis methods described in Sections 4.1−4.3 has allowed us to obtain an estimation of the fraction $x_i$ of the three phases for the aged samples (Cu2.4, Cu7.5, and Cu9.0) activated at RT (Table 1) and so achieve the first goal of this work. It is worth noting that the sum of the three $x_i$ values (last column in Table 1) is always close to the expected 1.0 value, the excess being always under the 10% of reliability, which is the typical error associated with the coordination number estimated with EXAFS. The aluminate phase being unreactive, it is interesting to know how the reactive phase is sheared between copper chloride and paratacamite. This datum is reported in Table 2, where $x_2$ and $x_3$ have been normalized to $(x_2 + x_3)$. It is important to note how the fraction of paratacamite and copper chloride follow the same trend obtained with solubility testing by Leofanti et al., see Figure 6 in ref 20. The EXAFS study presented here represents further

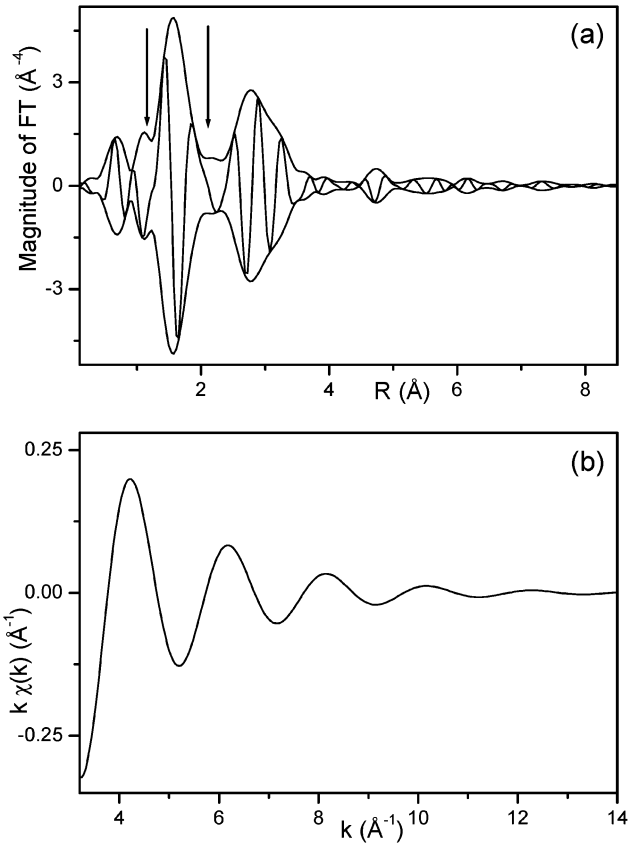


**Figure 5.** (a): $k^3$-weighted, phase-uncorrected, FT of the raw EXAFS signal of paratacamite reported: modulus (full line) and imaginary part (dotted line). The two arrows indicate the $R$-range used to extract the filtered first shell signal of paratacamite model compound reported in part (b).

**TABLE 1: Copper Atomic Fractions of the Three Phases (Cu-aluminate, paratacamite, $CuCl_2$) Present in the Cu9.0, Cu7.5, and Cu2.4 Catalysts (6 month aged) as Evaluated by EXAFS Data Analysis[a]**

| sample | Cu-aluminate $x_1$ | paratacamite $x_2$ | $CuCl_2$ $x_3$ | total |
|---|---|---|---|---|
| Cu2.4 | 0.66 | $0.37 \pm 0.05$ | $0.9 \pm 0.05$ | $1.06 \pm 0.07$ |
| Cu7.5 | 0.21 | $0.48 \pm 0.04$ | $0.32 \pm 0.03$ | $1.01 \pm 0.05$ |
| Cu9.0 | 0.18 | $0.52 \pm 0.06$ | $0.37 \pm 0.04$ | $1.07 \pm 0.07$ |

[a] The fraction of Cu-aluminate has been fixed according to what was learned in ref 19, see text. The last column represents the sum of the fraction of the three phases optimized in EXAFS fit procedure.

**TABLE 2: Relative Fraction of Paratacamite and Copper Chloride for Cu9.0, Cu7.5, and Cu2.4 Catalysts[a]**

| sample | paratacamite | $CuCl_2$ |
|---|---|---|
| Cu2.4 | 0.80 | 0.20 |
| Cu7.5 | 0.60 | 0.40 |
| Cu9.0 | 0.58 | 0.42 |

[a] Data obtained from the re-normalization of the fractions reported in Table 1.

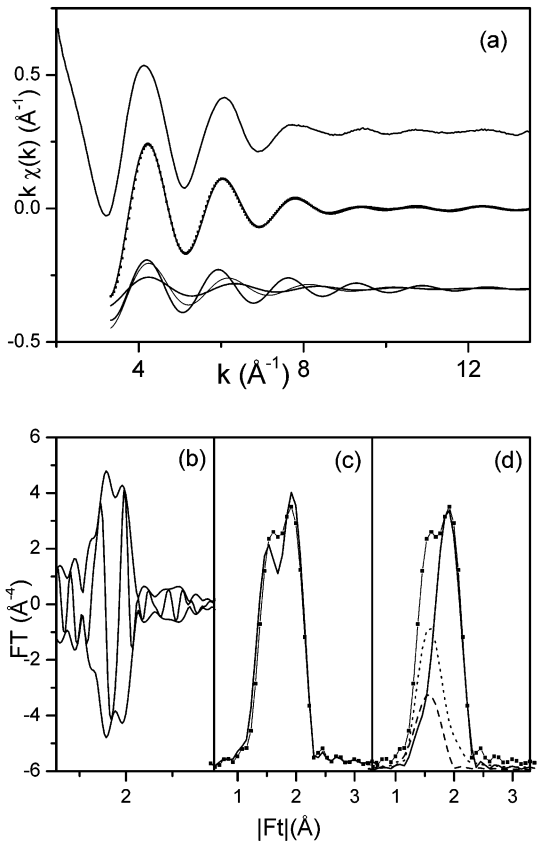


**Figure 6.** (a) From the top to the bottom: raw EXAFS data, first shell filtered data (scattered dots) and superimposing best fit (full line) obtained for the sample Cu7.5 activated at 300 K, the three optimized components of the three phases used in the fit (Cu-aluminate, paratacamite, copper chloride). (b) $k^3$-weighted, phase-uncorrected, FT of the raw EXAFS signal of the experimental signal reported in part (a): modulus (full line) and imaginary part (dotted line). (c) Experimental signal (scattered dots) and best fit (full line) in *R* space. (d) Contribution in *R* space ($k^3$-weighted) of the individual components optimized in the fit: Cu-aluminate (dashed line), paratacamite (dotted line), and copper chloride (full line). For comparison, also the $k^3$-weighted FT of the experimental EXAFS data is reported (scattered dots).

proof that the rate of transformation of copper chloride in paratacamite is related to the amount of copper present on the catalyst: the higher is the copper content, the slower is the transformation rate. This observation is in agreement with the hypothesis suggested by Zipelli et al.[11] that the conversion of copper chloride into paratacamite is likely catalyzed by surface Brønsted basic sites of $\gamma$-alumina. The reaction can be schematized as follows:

$$2CuCl_2 + 3(>Al-OH) \rightarrow Cu_2(OH)_3Cl + 3(>Al-Cl) \quad (3)$$

and can be favored by the presence of water, that can take part in the reaction either directly or, more probably, indirectly, by restoring the already reacted [OH] groups.

The quality of the fits obtained according this procedure can be appreciated in Figure 6 for sample Cu7.5. Part (a) reports, in the k space, from the top to the bottom the raw EXAFS signal, the first shell filtered signal superimposed at the simulated one and the three separated components coming from the three different phases. Parts (b), (c), and (d) report the $k^3$-weighted, phase uncorrected, FT of the signals reported in part (a).

**4.5. The Effect of the Activation Temperature.** The second aim of the present study is to prove that the thermal activation, under dynamic vacuum, implies the gradual inverse transformation of paratacamite in anhydrous copper chloride. From the $k^3$-weighted, phase-uncorrected, FT of sample Cu7.5 activated at 300, 393, and 473 K (vide supra Figure 2). Even a superficial view on the curves reported in Figure 2, the progressive decrement of Cu−O component (around 1.5 Å) and the parallel increase of the Cu−Cl component (around 2.00 Å) upon increasing the activation temperature is clearly visible.[42] Note the decrement of Cu−O is not total in consequence of the existence of a fraction of Cu species in the aluminate phase. This just represents a qualitative demonstration of the conversion of the $Cu_2(OH)_3Cl$ in $CuCl_2$.

**TABLE 3: Copper Atomic Fraction of the Three Phases (Cu-aluminate, paratacamite, $CuCl_2$) Present in the Cu7.5 Catalyst as a Function of the Activation Temperature As Evaluated by EXAFS Data Analysis[a]**

| activation (K) | aluminate $x_1$ | paratacamite $x_2$ | $CuCl_2$ $x_3$ | total |
|---|---|---|---|---|
| 300 | 0.21 | $0.48 \pm 0.04$ | $0.32 \pm 0.03$ | $1.01 \pm 0.05$ |
| 393 | 0.21 | $0.08 \pm 0.01$ | $0.73 \pm 0.07$ | $1.02 \pm 0.07$ |
| 473 | 0.21 | 0 | $0.84 \pm 0.09$ | $1.05 \pm 0.09$ |

[a] The fraction of Cu-aluminate has been fixed according to what was learned in ref 19, see text. The last column represents the sum of the fraction of the three phases optimized in EXAFS fit procedure.

The methodology described in Sections 4.1−4.3 can be applied to these data to allow the quantitative evaluation of the copper chloride and paratacamite phases. Table 3 reports the quantitative result obtained by EXAFS data analysis on three samples. It is appreciable that just a treatment at 393 K is enough to reduce the fraction of paratacamite from 48% to the 8% and the treatment at 473 K implies the total decomposition of $Cu_2(OH)_3Cl$ to form anhydrous $CuCl_2$.

**4.6. XANES Spectra Simulation: A Qualitative Study.** Also XANES spectroscopy can be used to determine the local environment of the adsorbing atom. Programs such as FEFF8,[43] CONTINUUM,[44] or MXAN[45] are able to reproduce a theoretical XANES spectrum starting from a cluster of atoms mimicking the local environment of the absorbing atom.[46−48] However, in the present case, this approach cannot be used owing to the amorphous nature of the highly dispersed $CuCl_2$ phase[19−24] that does not allow the construction of a meaningful cluster.

An alternative way is to use model compounds[24,49−51] and to try to reproduce each experimental XANES spectrum as the linear combination of the signals of the separate *F* phases. To do that, the XANES spectra of all samples and of all separated phases have to be interpolated in order to allow an estimation of the XANES intensity for all spectra at the same mesh of energies ($E_i$, $j = 1...N$) for direct comparison. Once this has been done, a theoretical spectrum can be generated as follow:

$$\mathrm{XANES}^{\mathrm{Theor}}(E_j, x_1, x_2, x_3) = \sum_{i=1}^{F} x_i \mathrm{XANES}^{F_i}(E_j) \quad (4)$$

The so obtained theoretical XANES spectrum depends on the hypothesized composition of the sample, i.e., on the values assumed by the parameters $x_i$ which are allowed to vary between 0 and 1 with the additional constraint that $\sum_{i=1}^{F} x_i = 1$. The optimum set of $x_i$ parameters is that able to minimize the function $\mathbf{F}(x_1, x_2, ...x_F)$, defined as the sum over all sampled points of the squared difference between the theoretical and the

experimental XANES spectra:[52]

$$\mathbf{F}(x_1, x_2, ...x_F) = \sum_{i=1}^{N}[\mathrm{XANES}^{\mathrm{Exp}}(E_i) - \mathrm{XANES}^{\mathrm{Theor}}(E_i)]^2 \quad (5)$$

If the number of the phases $F$ and their nature is unknown, then the principal component factor analysis (PCA) method, applied by Fernandez-Garcia et al.[53] to XANES spectroscopy is welcome. PCA is, in fact, able to identify and quantify the phases present along a series of samples. The PCA method has, however, not been used in the present case for two main reasons. First, we already know, from other techniques independent from XANES, that three phases are present.[19−24] Second, the PCA method being based on a statistical approach, its use on a set of only three spectra is borderline, if not misleading.

In the present case, eq 4 simply yields

$$\mathrm{XANES}^{\mathrm{Theor}}(E_i, x_1, x_2) = x_1\,\mathrm{XANES}^{\mathrm{Aluminate}}(E_i) + x_2\,\mathrm{XANES}^{\mathrm{Paratacamite}}(E_i) + (1 - x_1 - x_2)\,\mathrm{CuCl_2\ phase} \quad (6)$$

As was the case for the EXAFS study, the XANES spectrum of the Cu1.4 sample has been used as a model for the copper-aluminate phase. Owing to the large size of paratacamite crystal formed on the aged catalysts, very visible by XRD,[20] the XANES spectrum of the paratacamite model compound is very representative of the paratacamite phase present on the samples. Unfortunately, this does not hold for the $CuCl_2$ phase, which is highly dispersed on the catalyst.[20,22] This aspect represents the weakness of the XANES method here described (eqs 5 and 6) in the specific case of the $CuCl_2/\gamma$-$Al_2O_3$ catalyst. The use of a bulk material as model compound to reproduce the XANES spectrum of a highly dispersed phase is critical, because the relatively long mean free path of a few eV photoelectrons makes the XANES features affected by the location of several coordination shells around the adsorbing atom. In the present case, we are really dealing with a highly dispersed phase since, from chemisorption experiments,[22] we have found, for the Cu9.0 catalyst, that the fraction of 38% of the Cu atoms of the copper chloride phase are surface atoms. Moreover, this fraction depends on the Cu loading and on the activation temperature, causing a partial sintering process. These considerations explain why the quality of the XANES fits was poor (spectra not reported) when bulk $CuCl_2$ was used as a model. Note that for the EXAFS case, where only the first shell has been considered, this problem was negligible.

To partially overcome this problem, a model compound of highly dispersed $CuCl_2$ must be used. The most suitable material is a sample prepared using a double impregnation method. First, the $\gamma$-$Al_2O_3$ support has been impregnated by $MgCl_2$ to saturate the cationic vacancies at the alumina surface by $Mg^{2+}$ cations. Then the excess of $MgCl_2$ was washed, and the impregnation with $CuCl_2$ (5 wt %) is finally performed. In such a way this sample, measured after activation at 473 K, can be considered, in the first approximation, as a model compound of highly dispersed $CuCl_2$ phase. The use of this sample as a model to reproduce the copper chloride phase for all the catalysts here discussed (see Tables 1 and 3) introduces the following systematic errors in the fitting procedure: we will neglect the effect of both Cu loading and activation temperature on the size distribution of the $CuCl_2$ particles, and we will neglect the interaction between supported $CuCl_2$ particles and support, which is a Mg-aluminate and no more a Cu-aluminate.

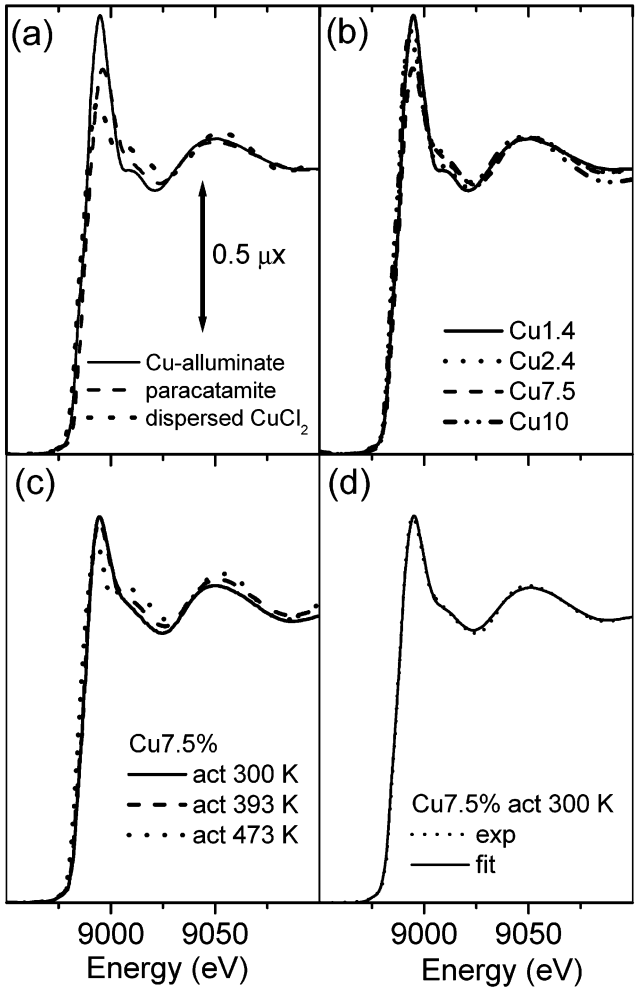


**Figure 7.** Normalized XANES spectra in the 8950−9100 eV range. (a) Copper-aluminate, paratacamite, and highly dispersed $CuCl_2$ (see text) model compounds, full dotted and dashed line, respectively. (b) Evolution of the XANES feature as a function of the copper content for catalysts activated at room temperature: Cu1.4 (full line), Cu2.4 (dotted line), Cu7.5 (dashed line), and Cu9.0 (dot−dashed line). (c) Evolution of the XANES feature of the Cu7.5 catalyst as a function of the activation temperature: 300 K (full line), 393 K (dashed line, and 473 K (dotted line). (d) Comparison between the experimental (full line) and the fitted XANES (dashed line) spectra. The latter has been obtained with $x_1 = 0.25$, $x_2 = 0.41$, and $x_3 = 0.34$.

Figure 7a reports the normalized XANES spectra, in the 8950−9100 eV range, of the three model compounds used to reproduce the spectra of the catalysts as a function of copper loading and temperature activation. The white line is a feature that allows easy discrimination among the three phases: its intensity moves from 1.47 (copper-aluminate, full line) through 1.29 (paratacamite, dashed line) to 1.18 (highly dispersed $CuCl_2$, dotted line), while its position exhibits a 2.8 eV blue-shift by moving from highly dispersed $CuCl_2$ to paratacamite. Also the features appearing in the 9000−9030 eV range are markedly different for the three compounds. The maximum of the first EXAFS oscillation occurs around 9048 eV for both Cu-aluminate and paratacamite, being around 9053 eV for the highly dispersed $CuCl_2$ phase.

Coming to the aged catalysts activated at 300 K, Figure 7b reports the evolution of the XANES feature as a function of the copper content for catalysts. The increase of the copper content causes a progressive decrease of the white line intensity, from 1.47 for Cu1.4 (full line) to 1.30 for Cu9.0 (dot−dashed

line), reflecting an increase of the paratacamite phase with respect to the Cu-aluminate phase. Appreciable modification of the 9000−9030 eV region is also observed, while no significant changes are observed in the position of the maximum of the first EXAFS oscillation, reflecting the minor fraction of the highly dispersed $CuCl_2$ phase in these samples. Figure 7c shows the evolution of the XANES feature of the Cu7.5 catalyst as a function of the activation temperature: 300 K (full line), 393 K (dashed line), and 473 K (dotted line). In this case, the progressive blue-shift of the maximum of the first EXAFS oscillation is observed upon increasing the activation temperature, reflecting the progressive transformation of paratacamite into highly dispersed $CuCl_2$. Also, the white line undergoes a progressive red-shift (1.8 eV) and a further reduction, down to 1.21 for the samples activated at 473 K, being the highly dispersed $CuCl_2$ phase that is characterized by the lowest white line intensity, see Figure 7a. Important modifications of the 9000−9030 eV region are also observed.

Even under the strong approximations discussed above, the quality of the fits obtained using the highly dispersed $CuCl_2$ phase for modeling the $XANES^{CuCl_2}(E_i)$ spectrum is strongly improved with respect to that obtained with bulk $CuCl_2$. An example of the obtained fits is reported in Figure 7d, where the experimental spectrum of Cu7.5 catalyst activated at 300 K (full line) is reported together with the theoretical spectrum obtained with the optimized values of the parameters: $x_1 = 0.25$, $x_2 = 0.41$, and $x_3 = 1 - (x_1 + x_2) = 0.34$. Along the whole set of samples, the optimized values of $x_1$, $x_2$, and $x_3$, constrained to $1 - (x_1 + x_2)$ agrees with those obtained from the EXAFS data analysis (Tables 1 and 3) within 2 esd. We consider this agreement only as qualitative since, as discussed above, our previous chemisorption study[22] has demonstrated that the size distribution of the $CuCl_2$ particles is determined by both Cu loading and activation temperature, so that it is virtually impossible to have the "perfect" XANES model for this phase in each sample.

As a consequence, we can conclude that the XANES study supports qualitatively the EXAFS data analysis, which is the most reliable technique for the quantitative determination of the three phases. It is, however, clear that, in any other cases where well-defined model can be available for all phases, the joint use of both EXAFS and XANES analyses here proposed will be of great help in material science for the analysis of mixed-phase samples.

## 5. Conclusions

We have used the case of the $CuCl_2/Al_2O_3$ material, which represents the basic catalyst for the ethylene oxychlorination reaction, to describe a generalization of the standard EXAFS procedure that can be of general interest in all cases where the absorbing species is present in more than one phase. This methodology has allowed us to quantify the fraction of copper species in the Cu-aluminate, copper chloride, and paratacamite ($Cu_2(OH)_3Cl$) phases as a function of copper loading and activation temperatures. Owing to the absence of a "perfect" XANES model for the highly dispersed $CuCl_2$ phase, the parallel XANES study could support the present EXAFS analysis on qualitative ground only. We have presented a methodology of general validity that allows us to extract quantitative information from EXAFS and XANES data collected on complex samples where the absorbing species is present in more than one phase, in order to have a reliable EXAFS and XANES spectrum of each separated phase.

**Acknowledgment.** We are strongly indebted to F. Bonino, A. Gabanotto, and F. Villain for their relevant and friendly support during EXAFS measurements. E. Giamello and G. Turnes Palomino are acknowledged for fruitful discussion.

## References and Notes

(1) Garilli, M.; Fatutto, P. L.; Piga, F. *Chim. Ind.* **1998**, *80*, 333.
(2) (a) McPherson, R. W.; Starks, C. M.; Fryar G. J. *Hydrocarbon Process.* **1979**, 75; (b) Naworski, J. S.; Evil, E. S. *Appl. Ind. Catal.* **1983**, *1*, 239.
(3) Mross, W. D. *Catal. Rev. Sci. Eng.* **1983**, *25*, 591.
(4) (a) Arcoya, A.; Cortes, A.; Seoane, X. L. *Can. J. Chem. Eng.* **1982**, *60*, 55. (b) Vetrivel, R.; Rao, K. V.; Seshan, K.; Krishnamurthy, K. R.; Prasada Rao, T. S. R. *Proc. 9th Int. Congr. Catal., Calgary* **1988**, *5*, 1766.
(5) Blanco, J.; Fayos, J.; Garcia De La Banda, J. F.; Soria, J. *J. Catal.* **1973**, *31*, 257.
(6) Avila, P.; Blanco, J.; Garcia-Fierro, J. L.; Mendioroz, S.; Soria, J. *Stud. Surf. Sci. Catal.* **1981**, *7B*, 1031.
(7) Baiker, A.; Monti, D.; Wokaun, A. *Appl. Catal.* **1986**, *23*, 425.
(8) Sermon, P. A.; Rollins, K.; Reyes, P. N.; Lawrence, S. A.; Martin Luengo, M. A.; Davies, M. J. *J. Chem. Soc., Faraday Trans. 1* **1987**, *83*, 1347.
(9) Garcia, C. L.; Resasco, D. E. *Appl. Catal.* **1989**, *46*, 251.
(10) Valle, J.; Vargas, A.; Ferreira, J. M.; Flores, A.; Novaro, A. *Stud. Surf. Sci. Catal.* **1981**, *7B*, 1040.
(11) Zipelli, G.; Bart, J. C.; Petrini, G.; Galvagno, S.; Cimino, C. *Z. Anorg. Allg. Chem.* **1983**, *502*, 199.
(12) Fortini, E. M.; Garcia, C. L.; Resasco, D. E. *J. Catal.* **1986**, *99*, 12.
(13) Sai Prasad, P. S.; Kanta Rao, P. *J. Chem. Soc., Chem. Commun.* **1987**, 951.
(14) Rouco, A. J. *Appl. Catal. A* **1994**, *117*, 139.
(15) Ott, R. J.; Baiker, A. *Stud. Surf. Sci. Catal.* **1982**, *16*, 685.
(16) Baiker, A.; Holstein, W. L. *J. Catal.* **1983**, *84*, 178.
(17) Bond, G. C.; Namijo, S. N.; Wakeman, J. S. *J. Mol. Catal.* **1991**, *64*, 305.
(18) (a) Dotson, R. L. *J. Catal.* **1974**, *33*, 210. (b) Hall, P. G.; Heaton, P.; Rosseinsky, D. R. *J. Chem. Soc., Faraday Trans. 1* **1984**, *80*, 2785. (c) Garcia, C. L.; Resasco, D. E. *J. Catal.* **1990**, *122*, 151.
(19) Leofanti, G.; Padovan, M.; Garilli, M.; Carmello, D.; Zecchina, A.; Spoto, G.; Bordiga, S.; Turnes Palomino, G.; Lamberti, C. *J. Catal.* **2000**, *189*, 91.
(20) Leofanti, G.; Padovan, M.; Garilli, M.; Carmello, D.; Marra, G. L.; Zecchina, A.; Spoto, G.; Bordiga, S.; Lamberti, C. *J. Catal.* **2000**, *189*, 105.
(21) Garilli, M.; Carmello, D.; Cremaschi, B.; Leofanti, G.; Padovan, M.; Zecchina, A.; Spoto, G.; Bordiga, S.; Lamberti, C. *Stud. Surf. Sci. Catal.* **2000**, *130*, 1917.
(22) Leofanti, G.; Marsella, A.; Cremaschi, B.; Garilli, M.; Zecchina, A.; Spoto, G.; Bordiga, S.; Fisicaro, P.; Berlier, G.; Prestipino, C.; Casali, G.; Lamberti, C. *J. Catal.* **2001**, *202*, 279.
(23) Leofanti, G.; Marsella, A.; Cremaschi, B.; Garilli, M.; Zecchina, A.; Spoto, G.; Bordiga, S.; Fisicaro, P.; Prestipino, C.; Villani, F.; Lamberti, C. *J. Catal.* **2002**, *204*, 375.
(24) Lamberti, C.; Prestipino, C.; Bonino F.; Capello, L.; Bordiga, S.; Spoto, G.; Zecchina, A.; Diaz Moreno, S.; Cremaschi, B.; Garilli, M.; Marsella, A.; Carmello, D.; Vidotto S.; Leofanti, G. *Angew. Chem., Int. Ed.* **2002**, *41*, 2341.
(25) Neurock, M.; Zhang, X.; Olken, M.; Jones, M.; Hickman, D.; Calverley, T.; Gulotty, R. *J. Phys. Chem. B* **2001**, *105*, 1562.
(26) Moonen, J.; Slot, J.; Lefferts, L.; Bazin, D.; Dexpert, H. *Physica B* **1995**, *208* & *209*, 689.
(27) Turnes Palomino, G.; Bordiga, S.; Zecchina, A.; Marra, G. L.; Lamberti, C. *J. Phys. Chem. B* **2000**, *104*, 8641.
(28) Lamberti, C.; Prestipino, C.; Bordiga, S.; Fitch, A. N.; Marra, G. L. *Nucl. Instrum. Methods B* **2003**, *200*, 155.
(29) Lamberti, C.; Zecchina, A.; Bordiga, S.; Spoto, G.; Leofanti, G.; Garilli, M. Proposal CK 017-00 LURE, Orsay (F), XAFS13 (D42), September 11−15, 2000.
(30) Lamberti, C.; Bordiga, S.; Salvalaggio, M.; Spoto, G.; Zecchina, A.; Geobaldo, F.; Vlaic, G.; Bellatreccia, M. *J. Phys. Chem. B* **1997**, *101*, 344.
(31) Michalowicz, A. *J. Phys. IV* (*France*) **1997**, *7*, C2−235.
(32) (a) Lytle, F. W.; Sayers, D. E.; Stern, E. A. *Physica B* **1989**, *158*, 701. (b) Durham, P. J. In *X-ray Absorption*; Koningsberger, D. C., Prins, R., Eds.; Wiley & Sons: New York, 1988; p 53.
(33) Burns, P. C.; Hawthorne, F. C. *Am. Mineral.* **1993**, *78*, 187.
(34) Restori, R.; Schwarzenbach, D. *Acta Crystallogr. B* **1986**, *42*, 201.
(35) Brownstein, S.; Han, N. F.; Gabe, E.; LePage, Y. *Z. Kristall.* **1989**, *189*, 13.
(36) Fleet, M. E. *Acta Crystallogr. B* **1975**, *31*, 183.

(37) Engberg, A. *Acta Chim. Scand.* **1970**, *24*, 3510.

(38) $N_i$ and $N_{\mathrm{fit}\,i}$ coincide in the case of a single chemical species: $x_i = 1.0$, see eq 2.

(39) The second phase has been simulated as anhydrous copper chloride because it was demonstrated that the degassing treatment at RT, performed in order to eliminate adsorbate, implies the losses of crystallization water from $CuCl_2 \cdot 2H_2O$.

(40) Giamello, E.; Murphy, D.; Magnacca, G.; Morterra, C.; Shioya, Y.; Nomura, T.; Anpo, M. *J. Catal.* **1992**, *136*, 510.

(41) Zhou, R.-S.; Snyder, R. L. *Acta Crystallogr. B* **1991**, *47*, 617.

(42) It is worth to note that the intensity of the Cu−Cl peak in the FT of the sample activated at 473 K is lower than the one activated at 393 K (Figure 2). This effect is due to a partial increase of the disorder in the local environment around copper caused by thermal activation (see ref 22).

(43) Ankudinov, A. L.; Rave, L. B.; Rehr, J. J.; Conradson, S. D. *Phys. Rev. B* **1998**, *58*, 7565.

(44) Tyson, T. A.; Hodgson, K. O.; Natoli, C. R.; Benfatto, M. *Phys. Rev. B* **1992**, *46*, 5997.

(45) Benfatto, M.; Della Longa, S.; Natoli, C. R. *J. Synchrotron Radiat.* **2003**, *10*, 51.

(46) Natoli, C. R.; Benfatto, M.; Della Longa, S.; Hatada, K. *J. Synchrotron Radiat.* **2003**, *10*, 26, and references therein.

(47) (a) Joly, Y.; Cabaret, D.; Renevier, H.; Natoli, C. R. *Phys. Rev. Lett.* **1999**, *82*, 2398. (b) Gotte, V.; Goulon, J.; Goulon-Ginet, C.; Rogalev, A.; Natoli, C. R.; Perie, K.; Barbe, J. M.; Guilard, R. *J. Phys. Chem. B* **2000**, *104*, 1927. (c) Wu, Z. Y.; Xian, D. C.; Natoli, C. R.; Marcelli, A.; Paris, E.; Mottana, A. *Appl. Phys. Lett.* **2001**, *79*, 1918.

(48) Lamberti, C.; Turnes Palomino, G.; Bordiga, S.; Berlier, G.; D'Acapito, F.; Zecchina, A. *Angew. Chem., Int. Ed.* **2000**, *39*, 2138.

(49) Lamberti, C.; Spoto, G.; Scarano, D.; Pazé, C.; Salvalaggio, M.; Bordiga, S.; Zecchina, A.; Turnes Palomino, G.; D'Acapito, F. *Chem. Phys. Lett.* **1997**, *269*, 500.

(50) (a) Garcia, J.; Blasco, J.; Sanchez, M. C.; Proietti, M. G.; Subias, G. *Surf. Rev. Lett.* **2002**, *9*, 821. (b) Subias, G.; Garcia, J.; Sanchez, M. C.; Blasco, J.; Proietti, M. G. *Surf. Rev. Lett.* **2002**, *9*, 1071.

(51) Kim, W. B.; Choi, S. H.; Lee, J. S. *J. Phys. Chem. B* **2000**, *104*, 8670.

(52) Lamberti, C.; Bordiga, S.; Cerrato, G.; Morterra, C.; Scarano, D.; Spoto, G.; Zecchina, A. *Comput. Phys. Commun.* **1993**, *74*, 119. (b) Lamberti, C.; Morterra, C.; Bordiga, S.; Cerrato, G.; Scarano, D. *Vib. Spectrosc.* **1993**, *4*, 273.

(53) Fernandez-Garcia, M.; Marquez Alvarez, C.; Haller, G. L. *J. Phys. Chem.* **1995**, *99*, 12565.